Asymptotic analysis of tracer diffusivity in nonadsorbing polymer solutions

Tai-Hsi Fan,[1] Bin Xie,[1] and Remco Tuinier[2]
[1]*Department of Mechanical Engineering, University of Connecticut, Storrs, Connecticut 06269-3139, USA*
[2]*Forschungszentrum Jülich, Institut für Festkörperforschung, Soft Matter, D-52425 Jülich, Germany*
(Received 13 August 2007; revised manuscript received 18 October 2007; published 16 November 2007)

We present an asymptotic and scaling analysis of the long-time self-diffusivity of a Brownian spherical particle in dilute polymer solutions with nonadsorbing chains. The polymer depletion zone near the particle surface is described by a continuous polymer density profile. Hydrodynamics formulated by the modified Stokes equation with nonuniform viscosity is solved by a regular perturbation approximation using the Green function method. The asymptotes predict how polymer depletion alters the friction a spherical particle experiences during translational and rotational motion within a quiescent fluid. The analysis agrees very well with full numerical computation, which enables us to investigate the scaling law for the polymer-mediated retardation effect using a stretched exponential form that is commonly applied by experimentalists. The scaling exponents revealed are consistent with the nominal values from collected experiment observations.

DOI: 10.1103/PhysRevE.76.051405 PACS number(s): 82.70.Dd, 66.20.+d, 61.25.Hq

I. INTRODUCTION

Self-diffusion is a transport process due to random molecular motions excited by thermal fluctuations [1–3], which plays an important role affecting mass transport in many biological and colloidal systems. Being able to predict self-diffusivity is essential for advancing the fundamental understanding of particle transport in a microenvironment containing biopolymers such as DNA, actin, polysaccharide, globular protein, and macromolecular drugs. Self-diffusivity in a crowded environment strongly affects diffusion-limited reaction kinetics [4–6] and protein-protein association rates [7,8]. The crowding effect also complicates the stability and folding kinetics of proteins [9], and therefore will further influence proteins' self-diffusivity. From an application point of view, probing self-diffusivity is important for the development of a variety of polymer characterization methods and novel medical devices for diagnostic or therapeutic purposes such as the delivery of quantum dots and molecular beacons for cancer detection and microsurgery, and the use of biochips for fast drug screening.

In the zero-frequency limit, the long-time self-diffusivity of dilute Brownian particles can be accurately predicted by Fick's law. The translational mobility (inverse of the friction coefficient) is defined by the particle's moving velocity divided by the fluid drag force as if the particle is pulled through the fluid [2,10]. In a homogeneous fluid, the Brownian particle's self-diffusivity is characterized by the Stokes-Einstein relation. Similarly, the resistant shear force and torque are generated if the particle is rotating within the fluid. For the no-slip case, Kirchoff obtained the formula for the resulting torque already in 1876 [11], and the connection to rotational mobility and the rotational diffusivity was first documented by Debye [12]. However, in polymer solutions, such a prediction is not accurate because the particle's dynamics is strongly affected by the background polymer chains suspended in the medium or even more so by a fixed polymer network [13]. A recent study revealed that the multiscale viscosity has a crossover regime depending on the typical length scale in the crowded polymer environment [14]. Clearly, the hydrodynamics is complicated by the spatial and temporal scale involved, rendering both theoretical and experimental analysis of self-diffusivity fairly difficult and speculative.

To be able to explain how biomacromolecules such as proteins move in cells and how the complex internal structure of cells hinders transport of solutes like proteins, measurements for a broad range of biomolecules and colloidal particles through a variety of polymer solutions were performed extensively over the last few decades. Techniques that were used are tracer diffusion, photobleaching recovery, sedimentation, and dynamic light scattering; see, for example, Refs. [15–25]. These experimental studies have shown that when colloidal particles move through media containing nonadsorbing chains, the particles' mobility is actually larger than what would be expected based on the bulk viscosity. An important reason for that is because polymer chains tend to be away from the region surrounding the particle due to a loss of configuration entropy near the surface. This region is called the depletion zone. Such a depletion zone can reduce the viscous drag the particle experiences, and thus alters the particle's translational and rotational diffusivity [26,27]. In a more complicated scenario, when particles interact with each other, the overlap of depletion zones further introduces attraction between the particles due to the asymmetric distribution of the osmotic pressure [28–31]. Understanding depletion forces is critical in modulating dispersion stability and coagulation kinetics of colloidal systems and is relevant for several processes in food, pharmaceutical, and cosmetic industries. In microrheology [32–35] it is possible that the polymer depletion affects the frequency-dependent rheological properties of a complex fluid including polymer chains.

Early theoretical work including Ogston *et al.* [36], Cukier [37], and Ngai and Phillies [38] suggested an exponential scaling relation to explain the deviation of the effective viscosity from the bulk viscosity. Odijk [39] estimated protein transport in semidilute polymer solutions and proposed a generalized stretched exponential function based on many experimental studies. Experimentalists frequently use such stretched exponential functions; see, for instance, [17].

The stretched exponential function is empirical and has not been justified theoretically. Our theory presents a feasible test for the applicability of the stretched exponential form used in practice and serves as a reference for the design of new experiments. All of the scaling parameters in this paper are phenomenologically inferred. The dynamic similarity of the retardation behavior for the decoupled translational and rotational motion is controlled by the apparent depletion thickness and the bulk polymer concentration. Details are given in Sec. IV B.

Kang *et al.* [40,41] have studied translational diffusion of dilute spheres through a network of freely suspended hard rods. In their approach, the hydrodynamic interactions between the suspending polymer chains and the spherical particle are directly accounted for. An alternative route to tackle our problem is to translate the presence of the polymer chains in solutions surrounding the sphere into an effective viscosity profile. Rather than simplifying the concentration profile as we proposed recently [26,27], here we use a realistic polymer chain concentration, and hence a continuous viscosity profile near a spherical particle. We present a regular perturbation approximation for the resistance force the sphere experiences based on the modified Stokes equation. In the zero-frequency limit, the longest relaxation time in the polymer solution is assumed to be very short to such a degree that the depletion layer does not deform while the sphere is moving. For small particles it can be shown that this is a fair approximation [39]. Analytical solutions for fluid flow problems with nonuniform viscosity are rarely seen in the literature except for boundary layer problems that have similarity solutions. A few relevant models, using the series expansion method, were developed for quantifying ion mobility in a viscous fluid [42–44]. Here we use a regular perturbation technique and the Green function integral solution to resolve the local viscosity effect. Assisted by numerical verification, we found that the asymptotic solutions are accurate for a broad range of depletion thicknesses. The numerical results also confirmed that the asymptotic solutions in the dilute limit well complement the results obtained by the two-layer model we recently developed [27], which is applicable for particles with a thin depletion layer containing relatively small polymer chains. The full numerical calculation is extended to the more practical semidilute regime, for which we also analyze the scaling behavior of the retardation function based on Odijk's generalized form [39], and finally provide an approximation of the scaling law for the reduced tracer diffusivity in semidilute polymer solutions.

II. ASYMPTOTIC ANALYSIS

A. Modified Stokes system

The linearized equation of motion for the low Reynolds number fluid flow is given by

$$\nabla \cdot \boldsymbol{\tau} = 0, \quad \boldsymbol{\tau} = -p\boldsymbol{\delta} + \eta[\nabla \mathbf{v} + (\nabla \mathbf{v})^T], \tag{1}$$

where $\boldsymbol{\tau}$ is the total stress, p is the pressure, $\boldsymbol{\delta}$ is the Kronecker delta, η is the dynamic viscosity, superscript T denotes the transpose of a tensor, and $\nabla \mathbf{v} + (\nabla \mathbf{v})^T$ is two times the strain rate tensor. The fluid density variation in the polymer solution is negligible, and the velocity field is divergence free. Expanding the divergence term in Eq. (1) and taking into account the viscosity gradient and the continuity equation, $\nabla \cdot \mathbf{v} = 0$, we have

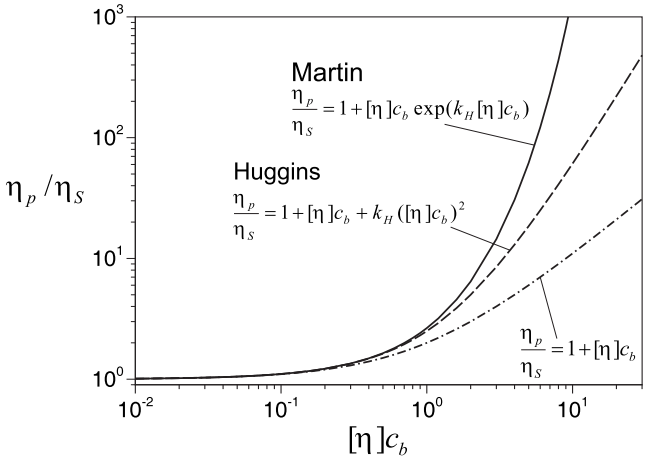

FIG. 1. Relative bulk viscosity η_p with respect to the solvent viscosity η_s vs bulk polymer concentration c_b following the Martin equation, Huggins equation, and the exact linear result $\eta_p = \eta_s(1 + [\eta]c_b)$ in dilute polymer solutions. Here k_H is the Huggins coefficient, which we set at a value of 0.5 that is at variance with experimental observations and $[\eta]$ is the intrinsic viscosity.

$$0 = -\nabla p + \eta\nabla^2 \mathbf{v} + \nabla \eta \cdot [\nabla \mathbf{v} + (\nabla \mathbf{v})^T], \tag{2}$$

where η is now a function of the local polymer concentration that varies with distance from the sphere surface. Next we shall specify the bulk viscosity of polymer solutions and the local viscosity near the particle surface. The bulk viscosity of a polymer solution η_p can be generally written as

$$\eta_p = \eta_s(1 + [\eta]c_b + \cdots), \tag{3}$$

where $[\eta]$ is the intrinsic viscosity that equals the hydrodynamic volume of a polymer chain in solution per unit mass and is close to $1/c_b^*$, with c_b^* the polymer overlap concentration. The higher concentration terms can be expressed in a general fashion as a function of $\epsilon = [\eta]c_b$. The semiempirical Martin equation can be used for correlating the bulk viscosity of polymer solutions up to high polymer concentrations [45]. This exponential form is consistent with the Huggins equation in the dilute regime (Fig. 1). For very dilute concentrations, a linear approximation is sufficient.

The local depletion effect is illustrated in Fig. 2. It is assumed that the polymer relaxation time is much faster than the particle motion time scale, and thus the depletion zone does not distort while the sphere is moving, that is, the Péclet number is small and the convective effect is negligible. Based on the mean-field approximation, de Gennes [46] derived an analytical concentration profile of polymer segments near a nonadsorbing planar wall for a semidilute polymer solution. The nonlinear concentration profile gradually increases from a vanishing value at the particle surface to the bulk value beyond the near-field regime [46,47]. The local

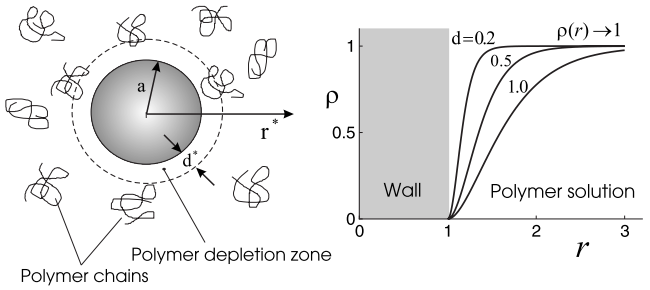

FIG. 2. Schematic picture of a solution with nonadsorbing chains around a spherical particle (left panel), and normalized polymer equilibrium concentration profiles ρ as a function of the radial distance r for various values of the characteristic depletion thickness d (right panel). Both r^* and d^* in the left panel are the corresponding dimensional values, respectively.

viscosity follows the polymer concentration distribution and also gradually increases from the surface to the bulk [48]. The one-dimensional nonlinear concentration profile is extended to a spherically symmetric surface [49], and has a general dimensionless form

$$\rho(r) = \left[r - 1 + \tanh\left(\frac{r-1}{d}\right)\right]^2 \Big/ r^2 \tag{4}$$

for the radial distance $1 \leqslant r = r^*/a < \infty$ (Fig. 2), where $\rho(r) = c(r)/c_b$, the normalized segment concentration, is the ratio of local polymer concentration $c(r)$ and the bulk concentration c_b, and $d = d^*/a$ is the dimensionless characteristic depletion thickness. Note that r and d are scaled by the particle radius a.

In the dilute limit the depletion thickness d^* is close to the polymer's radius of gyration [47], whereas in semidilute conditions, d^* is close to the correlation length [49]. The local viscosity $\eta(r)$ for a spherically symmetric system connects to the polymer concentration profile $\rho(r)$ as [48]

$$\eta(r) = \eta_s\{1 + [\eta]c_b\rho(r)e^{k_H[\eta]c_b\rho(r)}\}, \tag{5}$$

and thus in the dilute regime,

$$\eta(r) = \eta_s\{1 + [\eta]c_b\rho(r) + k_H([\eta]c_b\rho(r))^2 + \cdots\}. \tag{6}$$

In the bulk, where $\rho = 1$, Eqs. (5) and (6) are identical to the Martin and Huggins equations, respectively.

Intuitively, it is expected the effective viscosity η_{eff} lies in between the viscosities of pure solvent η_s and polymer solution η_p, and the corresponding Stokes-Einstein and Stokes-Einstein-Debye relations [22,25] can be modified by effective viscosities, formulated as $D^t_{\text{eff}} = k_BT/(6\pi\eta^t_{\text{eff}}a)$ and $D^r_{\text{eff}} = k_BT/(8\pi\eta^r_{\text{eff}}a^3)$, where D is self-diffusivity, k_BT is the thermal energy, and η^t_{eff} and η^r_{eff} are effective viscosities for translational and rotational motion, respectively. Our first goal is to find the viscosity correction functions g^t and g^r, defined as $\eta^t_{\text{eff}} = \eta_s g^t$ and $\eta^r_{\text{eff}} = \eta_s g^r$, so that the modified Stokes law and the decoupled translational and rotational Stokes-Einstein relations can be resolved.

B. Translational mode

The small, positive, and fixed dimensionless number ϵ, defined by $\epsilon = [\eta]c_b$, is selected for a regular expansion in the dilute limit. Substituting the continuous viscosity profile up to second order in concentration, $\eta \sim \eta_s(1 + \epsilon\rho + k_H\epsilon^2\rho^2)$, into the momentum equation, the second-order approximation of the Stokes equation can be written in a dimensionless form

$$0 \sim -\nabla p + \nabla^2\mathbf{v} + \epsilon[\rho\nabla^2\mathbf{v} + \nabla\rho\cdot(\nabla\mathbf{v} + (\nabla\mathbf{v})^T)] + \epsilon^2[k_H\rho^2\nabla^2\mathbf{v} + k_H\nabla\rho^2\cdot(\nabla\mathbf{v} + (\nabla\mathbf{v})^T)] \tag{7a}$$

for $1 \leqslant r < \infty$, provided the characteristic scales for length, velocity, stress field, and accordingly the total drag force $\mathbf{F}$ as

$$\text{length} \sim a, \quad \mathbf{v} \sim U, \quad \boldsymbol{\tau} \sim \eta_s U/a, \quad \mathbf{F} \sim \eta_s a U,$$

where a is the particle radius, $\mathbf{U} = U\hat{\mathbf{e}}_z$ is the translational velocity of the particle along the z axis, and η_s is the solvent viscosity corresponding to polymer concentration $\rho = 0$. The continuity equation is

$$\nabla\cdot\mathbf{v} = 0. \tag{7b}$$

In a quiescent fluid, the governing system is complemented by the no-slip and vanishing far-field boundary conditions:

$$v_r = \cos\theta, \quad v_\theta = -\sin\theta \text{ at } r = 1, \tag{8a}$$

$$v_r, \quad v_\theta \to 0, \quad \text{and } p \to 0 \text{ as } r \to \infty. \tag{8b}$$

The axisymmetric system can be simplified by the Stokes stream function $\psi(r,\theta)$ [10,50,51] using spherical polar coordinates (r,θ,φ), where θ denotes the polar coordinate and the flow pattern is symmetric in the azimuthal direction φ. The stream function $\psi(r,\theta)$ is related to the velocity field $\mathbf{v} = v_r\hat{\mathbf{e}}_r + v_\theta\hat{\mathbf{e}}_\theta$ by

$$v_r = \frac{-1}{r^2\sin\theta}\frac{\partial\psi}{\partial\theta}, \quad v_\theta = \frac{1}{r\sin\theta}\frac{\partial\psi}{\partial r}.$$

We now look for the perturbation solution in terms of power series in ϵ by a regular expansion of pressure, velocity, stream function, and vorticity, expressed as

$$p(r,\theta;\epsilon) \sim p_0 + \epsilon p_1 + \epsilon^2 p_2,$$

$$v_r(r,\theta;\epsilon) \sim v_{r0} + \epsilon v_{r1} + \epsilon^2 v_{r2},$$

$$v_\theta(r,\theta;\epsilon) \sim v_{\theta0} + \epsilon v_{\theta1} + \epsilon^2 v_{\theta2},$$

$$\psi(r,\theta;\epsilon) \sim \psi_0 + \epsilon\psi_1 + \epsilon^2\psi_2,$$

$$\boldsymbol{\zeta}(r,\theta;\epsilon) \sim \boldsymbol{\zeta}_0 + \epsilon\boldsymbol{\zeta}_1 + \epsilon^2\boldsymbol{\zeta}_2,$$

where $\boldsymbol{\zeta} = \nabla\times\mathbf{v}$ denotes the vorticity. For an axisymmetric system, it can be proven that the stream function ψ satisfies the following relation [50,51]:

$$-\nabla\times\nabla\times\boldsymbol{\zeta} = \frac{1}{r\sin\theta}E^4\psi\hat{\mathbf{e}}_\varphi, \tag{9}$$

where

$$E^4 \equiv \left[\frac{\partial^2}{\partial r^2} + \frac{\sin\theta}{r^2}\frac{\partial}{\partial\theta}\left(\frac{1}{\sin\theta}\frac{\partial}{\partial\theta}\right)\right]^2.$$

Substituting above expansions into Eqs. (7a), (7b), (8a), and (8b), and then equating the coefficients of the like powers of ϵ, the leading-, first-, and second-order systems can be written as

$O(\epsilon^0)$:

$$0 = \nabla \cdot \mathbf{v}_0,$$

$$0 = -\nabla p_0 + \nabla^2 \mathbf{v}_0,$$

$$v_{r0} = \cos\theta, \quad v_{\theta 0} = -\sin\theta, \quad \text{at } r = 1,$$

$$v_{r0}, v_{\theta 0} \to 0, \quad \text{and } p_0 \to 0 \quad \text{as } r \to \infty.$$

$O(\epsilon^1)$:

$$0 = \nabla \cdot \mathbf{v}_1,$$

$$0 = -\nabla p_1 + \nabla^2 \mathbf{v}_1 + \rho\nabla^2 \mathbf{v}_0 + \nabla\rho \cdot [\nabla \mathbf{v}_0 + (\nabla \mathbf{v}_0)^T],$$

$$v_{r1} = v_{\theta 1} = 0, \quad \text{at } r = 1,$$

$$v_{r1}, v_{\theta 1}, p_1 \to 0, \quad \text{as } r \to \infty.$$

$O(\epsilon^2)$:

$$0 = \nabla \cdot \mathbf{v}_2,$$

$$0 = -\nabla p_2 + \nabla^2 \mathbf{v}_2 + \rho\nabla^2 \mathbf{v}_1 + \nabla\rho \cdot [\nabla \mathbf{v}_1 + (\nabla \mathbf{v}_1)^T] + k_H \rho^2 \nabla^2 \mathbf{v}_0 + k_H \nabla\rho^2 \cdot [\nabla \mathbf{v}_0 + (\nabla \mathbf{v}_0)^T],$$

$$v_{r2} = v_{\theta 2} = 0, \quad \text{at } r = 1,$$

$$v_{r2}, v_{\theta 2}, p_2 \to 0, \quad \text{as } r \to \infty.$$

By applying the trial solution $\psi(r,\theta) = f(r)\sin^2\theta \sim \sin^2\theta(f_0 + \epsilon f_1 + \epsilon f_2)$ to the expansions and solving for the separated radial function $f(r)$, the leading-order system leads to the Stokes solution:

$$\psi_0 = \left(\frac{1}{4r} - \frac{3r}{4}\right)\sin^2\theta, \tag{10a}$$

$$\mathbf{v}_0 = \left(\frac{3}{2r} - \frac{1}{2r^3}\right)\cos(\theta)\hat{\mathbf{e}}_r - \left(\frac{3}{4r} + \frac{1}{4r^3}\right)\sin(\theta)\hat{\mathbf{e}}_\theta, \tag{10b}$$

$$p_0 = \frac{3\cos\theta}{2r^2}. \tag{10c}$$

The total drag force $\mathbf{F}$ is calculated by the viscous dissipation rate over the entire flow field induced by the moving particle, or by the area integration of the pressure and shear stress over the particle surface. The dimensionless result for the Stokes law [10] states $\mathbf{F} = -6\pi\hat{\mathbf{e}}_z$, where the negative sign shows that the force is opposite to the particle moving direction. We now proceed to resolve the first- and second-order systems.

1. First-order approximation

By taking the curl of the momentum equation of the first-order system and replacing $\rho\nabla^2\mathbf{v}_0$ by $\rho\nabla p_0$, we have

$$0 = \nabla \times \nabla^2 \mathbf{v}_1 + \nabla\rho \times \nabla p_0 + \nabla \times \{\nabla\rho \cdot [\nabla \mathbf{v}_0 + (\nabla \mathbf{v}_0)^T]\}.$$

Applying the vector identity, $\nabla^2\mathbf{v}_1 = \nabla(\nabla\cdot\mathbf{v}_1) - \nabla\times\nabla\times\mathbf{v}_1$, the first term on the right-hand side of the above equation can be replaced by $-\nabla\times\nabla\times\boldsymbol{\zeta}_1$, that equals $E^4\psi_1/(r\sin\theta)\hat{\mathbf{e}}_\phi$ in terms of the stream function. The second term reduces to $(\rho'/r)(\partial p_0/\partial\theta)\hat{\mathbf{e}}_\phi$. Because

$$\hat{\mathbf{e}}_r \cdot [\nabla \mathbf{v}_0 + (\nabla \mathbf{v}_0)^T] = 2e_{rr0}\hat{\mathbf{e}}_r + 2e_{\theta r0}\hat{\mathbf{e}}_\theta,$$

where e_{rr0} and $e_{\theta r0}$ are the strain rate components from the leading-order solution, the third term also has a component in the ϕ direction only. We thus simplify the momentum equation to a scalar equation for the unknown function ψ_1, expressed as

$$E^4\psi_1 = \rho'\sin\theta\left(\frac{\partial^2 v_{r0}}{\partial r\partial\theta} - r\frac{\partial^2 v_{\theta 0}}{\partial r^2} - \frac{\partial p_0}{\partial\theta}\right) + \rho''\sin\theta\left(v_{\theta 0} - r\frac{\partial v_{\theta 0}}{\partial r} - \frac{\partial v_{r0}}{\partial\theta}\right), \tag{11}$$

where the right-hand side is given by the leading-order solution, and ρ' and ρ'' are the first- and second-order r derivatives of the segment concentration profile defined by Eq. (4). Now substituting $\psi_1(r,\theta) = \sin^2(\theta)f_1(r)$, we obtain the separated fourth-order ordinary differential equation (ODE):

$$Lf_1 = h_1(r), \tag{12}$$

where

$$L \equiv \frac{d^4}{dr^4} - \frac{4}{r^2}\frac{d^2}{dr^2} + \frac{8}{r^3}\frac{d}{dr} - \frac{8}{r^4}$$

is self-adjoint and has variable coefficients being continuous in the interval $1 \leqslant r < \infty$. The nonhomogeneous term is given by

$$h_1(r) = \rho'\left(\frac{9}{2r^2} + \frac{3}{2r^4}\right) - \rho''\left(\frac{3}{2r^3}\right). \tag{13}$$

By taking θ and r derivatives of the stream function ψ_1, the first-order velocity field can be written as

$$\mathbf{v}_1 = \frac{-2\cos\theta}{r^2}f_1\hat{\mathbf{e}}_r + \frac{\sin(\theta)}{r}f_1'\hat{\mathbf{e}}_\theta. \tag{14}$$

From velocity boundary conditions we have

$$f_1(r) = 0 \text{ at } r = 1,$$

$$f_1'(r) = 0 \text{ at } r = 1,$$

$$f_1(r)/r^2 \to 0 \text{ as } r \to \infty,$$

$$f_1'(r)/r \to 0 \text{ as } r \to \infty. \tag{15}$$

Because the associated homogeneous boundary-value problem of Eq. (12) admits only a trivial solution, implying the

solution for f_1 exists and is unique, we can now look for f_1 in terms of the Green function integration solution. Details of the integral form and derivation of the Green function are given in the Appendix. The radial function for the first-order system can then be written as

$$f_1(\xi) = \int_1^{\xi} G_1(r,\xi)h_1(r)dr + \int_{\xi}^{\infty} G_2(r,\xi)h_1(r)dr, \quad (16)$$

where $h_1(r)$ is given by Eq. (13) and the Green functions are

$$G_1 = \frac{-r^4}{30\xi} + \frac{\xi}{6}r^2 + \frac{1}{12}\left(\frac{r}{\xi} + \frac{\xi}{r}\right) - \frac{\xi r}{4} - \frac{1}{20\xi r},$$

$$G_2 = \frac{-\xi^4}{30r} + \frac{r}{6}\xi^2 + \frac{1}{12}\left(\frac{\xi}{r} + \frac{r}{\xi}\right) - \frac{r\xi}{4} - \frac{1}{20r\xi}. \quad (17)$$

Note that both integrands in Eq. (16) are smooth functions within the corresponding interval.

2. Second-order approximation

By taking the curl of the second-order momentum equation and replacing the second-order velocity component by the stream function ψ_2, after a lengthy simplification process, the equation reduces to

$$Lf_2 = h_2(r) \text{ for } 1 \leqslant r < \infty, \quad (18)$$

where

$$h_2(r) = \frac{9\rho\rho'}{r^2}\left(k_H - \frac{1}{2}\right) + \frac{3\rho\rho'}{r^3}\left(\frac{1}{2} - k_H\right) - \frac{3k_H\rho'^2}{r^3} + \frac{3\rho\rho'}{r^4} \times\left(k_H - \frac{1}{2}\right) - \left(\frac{8\rho'}{r^3} + \frac{2\rho''}{r^2}\right)f_1 + \left(\frac{2\rho'}{r^2} + \frac{2\rho''}{r}\right)f_1' + \left(\frac{2\rho'}{r} - \rho''\right)f_1'' - 2\rho' f_1'''$$

depends on the lower-order solutions. Now considering the second-order velocity field,

$$\mathbf{v}_2 = \frac{-2\cos\theta}{r^2}f_2\hat{\mathbf{e}}_r + \frac{\sin(\theta)}{r}f_2'\hat{\mathbf{e}}_\theta, \quad (19)$$

the corresponding boundary conditions for f_2 are

$$f_2(r) = 0 \text{ at } r = 1,$$

$$f_2'(r) = 0 \text{ at } r = 1,$$

$$f_2(r)/r^2 \to 0 \text{ as } r \to \infty,$$

$$f_2'(r)/r \to 0 \text{ as } r \to \infty. \quad (20)$$

Therefore the unique solution for f_2 can be expressed as

$$f_2(\xi) = \int_1^{\xi} G_1(r,\xi)h_2(r)dr + \int_{\xi}^{\infty} G_2(r,\xi)h_2(r)dr \quad (21)$$

for $1 \leqslant r, \xi < \infty$, where the Green function is given by Eq. (17).

In summary, the perturbation approximation for the modified Stokes stream function and the velocity components are

$$\psi(r,\theta;\epsilon) = \psi_0 + \epsilon\psi_1 + \epsilon^2\psi_2 + \cdots \sim \sin^2\theta[f_0(r) + \epsilon f_1(r) + \epsilon^2 f_2(r)],$$

$$v_r(r,\theta,\epsilon) \sim \frac{-2\cos\theta}{r^2}[f_0(r) + \epsilon f_1(r) + \epsilon^2 f_2(r)],$$

$$v_\theta(r,\theta,\epsilon) \sim \frac{\sin\theta}{r}[f_0'(r) + \epsilon f_1'(r) + \epsilon^2 f_2'(r)],$$

where $f_0(r) = 1/4r - 3r/4$, $f_1(r)$ and $f_2(r)$ are given by Eqs. (16) and (21). We note that Leibniz's rule must be applied when taking differentiation of f_1 and f_2 with respect to r, and in the final results, the variables ξ and r have been switched to comply the expression using r as an independent variable.

3. Stress field and total drag force

Based on the second-order approximation described above, we further integrate the first- and second-order momentum equations and obtain the higher-order correction for the pressure field:

$$p_1(r,\theta) = \cos\theta\left(\frac{3\rho}{2r^2} - \frac{3\rho'}{2r^3} - \frac{4}{r^3}f_1 + \frac{2}{r^2}f_1' - f_1'''\right),$$

and

$$p_2(r,\theta) = \cos\theta\left\{\frac{3k_H\rho}{r^2}\left(\frac{\rho}{2} - \frac{\rho'}{r}\right) - \frac{2}{r^2}\left(\rho' + \frac{2\rho}{r}\right)f_1 + \frac{2}{r}\left(\rho' + \frac{\rho}{r}\right)f_1' - \rho' f_1'' - \rho f_1''' - \frac{4}{r^3}f_2 + \frac{2}{r^2}f_2' - f_2'''\right\}.$$

At $r=1$, ρ, ρ', G, and G' vanish. The corrected surface pressure can then be simplified to

$$p(1,\theta;\epsilon) = \frac{3}{2}\cos\theta\left[1 - \frac{2}{3}\epsilon\int_1^{\infty} G_2'''(\xi,1)h_1(\xi)d\xi - \frac{2}{3}\epsilon^2\int_1^{\infty} G_2'''(\xi,1)h_2(\xi)d\xi\right],$$

where the integration kernel

$$G_2'''(\xi,1) = -\frac{1}{2\xi} - \frac{\xi}{2}.$$

It can be proven that the normal stress σ_{rr} vanishes at $r=1$, and the shear stress $\sigma_{r\theta}$ at the particle surface reduces to

$$\sigma_{r\theta}(1,\theta;\epsilon) = \frac{3}{2}\sin\theta\left[1 + \frac{2}{3}\epsilon\int_1^{\infty} G_2''(\xi,1)h_1(\xi)d\xi + \frac{2}{3}\epsilon^2\int_1^{\infty} G_2''(\xi,1)h_2(\xi)d\xi\right],$$

where

$$G_2''(\xi,1) = -\frac{1}{2\xi} + \frac{\xi}{2}.$$

Surface integration of the local pressure and shear stress fields yields the dimensionless drag force, $F=|\mathbf{F}|=6\pi g^t$. Finally we can express the correction function g^t in terms of the Green function integral solution:

$$g^t = \frac{1}{3}\left[1 - \frac{2}{3}\epsilon\int_1^\infty G_2'''h_1 d\xi - \frac{2}{3}\epsilon^2\int_1^\infty G_2'''h_2 d\xi\right] + \frac{2}{3}\left[1 + \frac{2}{3}\epsilon\int_1^\infty G_2''h_1 d\xi + \frac{2}{3}\epsilon^2\int_1^\infty G_2''h_2 d\xi\right]. \quad (22)$$

It is clear that the leading-order solution is consistent with the Stokes law, in which the pressure contributes 1/3 and the shear force contributes another 2/3 to the total drag force. Because $G_2'''(\xi,1)<0$ and $G_2''(\xi,1)\geqslant 0$, both pressure (terms in the first bracket) and shear stress (terms in the second bracket) contributions to the total drag force increases as the polymer concentration increases; that is, the correction function $g^t \geqslant 1$. Although analytical integration of Eq. (22) does not exist except limiting cases, all integrands are smooth functions so that the full integration can be easily calculated by the standard quadrature method.

In the protein limit where the depletion thickness $d \gg 1$, the leading-order approximation of Eq. (4) reduces to

$$\rho(r) \simeq \left(\frac{r-1}{r}\right)^2\left(1+\frac{2}{d}\right). \quad (23)$$

Substituting into $h_1(r)$ and $h_2(r)$, and then completing the integrations in Eq. (22), the closed-form second-order approximation for g^t leads to a simple algebraic form:

$$g^t \simeq 1 + \frac{89}{210}\epsilon\left(1+\frac{2}{d}\right) + \frac{103\,600k_H - 26\,617}{44\,100}\epsilon^2\left(1+\frac{2}{d}\right)^2 \quad (24)$$

for $\epsilon \ll 1$ and $d \gg 1$. This resulting simple analytical expression provides the concentration dependence of the effective viscosity a small sphere experiences in a polymer solution. For $1/d \to 0$, $\eta_{\text{eff}}^t/\eta_s = g^t$ approaches $1+89\epsilon/210$ up to first order in polymer concentration. This means that in the very dilute limit the effective viscosity the small sphere experiences, η_{eff}^t, is significantly smaller than the macroscopic viscosity $\eta_p = \eta_s(1+\epsilon)$, whereas η_{eff}^t is still larger than η_s in the protein limit. Later in this paper we will show that the protein limit consists a different scaling behavior compared to the colloidal limit. This protein limit result is, as will be shown in Sec. IV B, also important for rescaling the exponential retardation factor in order to establish the scaling laws to be discussed in the results section.

C. Rotational mode

When a sphere is rotating in a quiescent fluid, the low Reynolds number flow is solely driven by the shear stress [12,27]. The second-order approximation of the dimensionless Stokes system is governed by Eqs. (7a) and (7b) except the vanishing pressure term. We have applied characteristic scales for length, velocity, shear stress and torque as follows:

$$\text{length} \sim a, \quad \mathbf{v} \sim \Omega a, \quad \boldsymbol{\tau} \sim \eta_s\Omega, \quad \mathbf{T} \sim \eta_s\Omega a^3,$$

where $\boldsymbol{\Omega}=\Omega\hat{\mathbf{e}}_z$ is the angular velocity with $\hat{\mathbf{e}}_z$ indicating the rotating axis, and $\mathbf{T}$ is the shear-induced torque on the sphere. The governing system, in terms of the spherical polar coordinates (r,θ,φ), is complemented by the no-slip and vanishing far-field boundary conditions: $v_\varphi = \sin\theta$ at $r=1$, and $v_\varphi = 0$ as $r\to\infty$, where φ is the azimuthal direction corresponding to the rotating axis. We now look for straightforward expansion of the velocity component v_φ in terms of a power series in ϵ, expressed as $v_\varphi(r,\theta;\epsilon) \sim v_{\varphi 0} + \epsilon v_{\varphi 1} + \epsilon^2 v_{\varphi 2}$. The resulting leading-, first-, and second-order solutions are listed below.

The leading-order system is

$$\nabla^2 v_{\varphi 0} - \frac{v_{\varphi 0}}{r^2\sin^2\theta} = 0,$$

$$v_{\varphi 0} = \sin\theta \quad \text{at } r=1,$$

$$v_{\varphi 0} \to 0 \quad \text{as } r\to\infty.$$

Substituting the trial solution, $v_{\varphi 0}(r,\theta)=\sin(\theta)w_0(r)$, the leading-order system reduces to an ODE for the unknown radial function w_0, written as $w_0''+(2/r)w_0'-(2/r^2)w_0=0$, for which the corresponding boundary conditions are $w_0=1$ at $r=1$, and $w_0=0$ as $r\to\infty$. The solution for the leading-order system (Stokes approximation) is $w_0=1/r^2$ and $v_{\varphi 0}=\sin(\theta)/r^2$. Following the leading-order result, the first-order system reduces to

$$\nabla^2 v_{\varphi 1} - \frac{v_{\varphi 1}}{r^2\sin^2\theta} = \frac{3\rho'\sin\theta}{r^3},$$

$$v_{\varphi 1} = 0 \quad \text{at } r=1,$$

$$v_{\varphi 1} \to 0 \quad \text{as } r\to\infty.$$

By substituting $v_{\varphi 1}=\sin(\theta)w_1(r)$ we obtain a nonhomogeneous self-adjoint second-order ODE,

$$r^2 w_1'' + 2rw_1' - 2w_1 = \frac{3\rho'}{r}, \quad (25)$$

with homogeneous boundary conditions: $w_1=0$ at $r=1$ and $w_1\to 0$ as $r\to\infty$. The unique Green function integral solution for w_1 is

$$w_1(\xi) = \int_1^\xi G_1(r,\xi)h_1(r)dr + \int_\xi^\infty G_2(r,\xi)h_1(r)dr \quad (26)$$

for $1\leqslant r,\ \xi < \infty$, where

$$h_1(r) = 3\rho'(r)/r, \quad (27)$$

and the Green functions for the corresponding domains become

$$G_1(r,\xi) = \frac{-r}{3\xi^2} + \frac{1}{3\xi^2 r^2} \quad \text{for } 1\leqslant r\leqslant\xi,$$

$$G_2(r,\xi) = \frac{-\xi}{3r^2} + \frac{1}{3\xi^2 r^2} \quad \text{for } \xi \leqslant r < \infty. \tag{28}$$

The following derivatives for the radial function $w(r)$ are required for solving the second-order system:

$$w_1'(r) = \int_1^r G_1'(\xi,r)h_1(\xi)d\xi + \int_r^\infty G_2'(\xi,r)h_1(\xi)d\xi,$$

and

$$w_1''(r) = \int_1^r G_1''(\xi,r)h_1(\xi)d\xi + \int_r^\infty G_2''(\xi,r)h_1(\xi)d\xi + \frac{h_1(r)}{r^2}.$$

Note that the field and source points are switched, and the h_1/r^2 term comes from the discontinuous property of the first derivative of the Green function at $\xi=r$. After a few algebraic operations, the second-order system reduces to

$$r^2 w_2'' + 2rw_2' - 2w_2 = h_2(r),$$

$$w_2 = 0 \quad \text{at } r = 1,$$

$$w_2 \to 0 \quad \text{as } r \to \infty,$$

where the differential operator and the Green function are the same as the first-order system. The nonhomogeneous term is

$$h_2(r) = \frac{6k_H\rho\rho'}{r} - \rho h_1 + (2\rho + \rho' r)\int_1^\infty G(\xi,r)h_1(\xi)d\xi - (2\rho r + \rho' r^2)\int_1^\infty G' h_1 d\xi - \rho r^2 \int_1^\infty G'' h_1 d\xi. \tag{29}$$

Clearly,

$$w_2(r) = \int_1^r G_1(\xi,r)h_2(\xi)d\xi + \int_r^\infty G_2(\xi,r)h_2(\xi)d\xi.$$

The only nonzero shear stress $\sigma_{\varphi r}$ can be derived by the approximated velocity field. At the particle surface, the shear stress becomes

$$\sigma_{\varphi r}(1,\theta;\epsilon) = \sin(\theta)\left[-3 + \epsilon\int_1^\infty G_2'(\xi,1)h_1(\xi)d\xi + \epsilon^2\int_1^\infty G_2'(\xi,1)h_2(\xi)d\xi\right],$$

where $G_2'(\xi,1) = -1/\xi^2$, and h_1 and h_2 are given by Eqs. (27) and (29). We conclude that the shear-induced torque on the rotating sphere is calculated by

$$\mathbf{T} = \int_{\partial\Omega} \mathbf{r} \times (\boldsymbol{\tau}\cdot\mathbf{n})dA = -8\pi g^r \hat{\mathbf{e}}_z,$$

where the correction factor for the rotational motion is

$$g^r = 1 + \frac{1}{3}\epsilon\int_1^\infty \frac{h_1(\xi)}{\xi^2}d\xi + \frac{1}{3}\epsilon^2\int_1^\infty \frac{h_2(\xi)}{\xi^2}d\xi. \tag{30}$$

In the protein limit, the segment concentration profile is given by Eq. (23) and the closed-form second-order approximation for g^r attains the simple form

$$g^r \simeq 1 + \frac{\epsilon}{10}\left(1 + \frac{2}{d}\right) + \frac{20k_H - 13}{700}\epsilon^2\left(1 + \frac{2}{d}\right)^2 \tag{31}$$

for $\epsilon < 1$ and $d \gg 1$. For $1/d \to 0$, $\eta_{\text{eff}}^r/\eta_s = g^r$ approaches $1 + \epsilon/10$ in the very dilute limit. The effective viscosity the small rotating sphere experiences, η_{eff}^r, is only perceptibly larger than the pure solvent viscosity and much smaller than the macroscopic viscosity $\eta_p = \eta_s(1+\epsilon)$.

III. NUMERICAL ANALYSIS

In this section we present a concise way to resolve the depletion effect on particle transport numerically in order to verify the asymptotic solution and to cover the calculation of the effective viscosity for a broader concentration range including the semidilute regime. Though a complete numerical simulation using any domain discretization method for a low Reynolds number flow seems doable for problems with nonuniform viscosity, the implementation is not trivial because the particle-induced fluid flow has long-range effects that require a computational domain of at least two orders of magnitude larger than the particle size. The numerical stiffness raised by the viscosity gradient across a thin depletion layer causes major difficulties in generating a well-converged solution. However, having an axisymmetric configuration one can avoid the full simulation by using the stream function formulation as follows.

A. Translational mode

Starting from taking the curl of the modified momentum equation, the pressure term is eliminated, and the second and third terms on the right-hand side of Eq. (2) reduce to

$$\boldsymbol{\nabla}\times(\eta\nabla^2\mathbf{v}) = -\eta\boldsymbol{\nabla}\times\boldsymbol{\nabla}\times\boldsymbol{\zeta} + \eta'\nabla^2 v_\theta \hat{\mathbf{e}}_\varphi + \frac{\eta'}{r^2}\left(2\frac{\partial v_r}{\partial\theta} - \frac{v_\theta}{\sin^2\theta}\right)\hat{\mathbf{e}}_\varphi,$$

and

$$\boldsymbol{\nabla}\times(\boldsymbol{\nabla}\eta\cdot[\boldsymbol{\nabla}\mathbf{v} + (\boldsymbol{\nabla}\mathbf{v})^T]) = \eta'\left(\frac{\partial^2 v_\theta}{\partial r^2} - \frac{1}{r}\frac{\partial^2 v_r}{\partial r\partial\theta}\right)\hat{\mathbf{e}}_\varphi + \eta''\left(\frac{\partial v_\theta}{\partial r} - \frac{v_\theta}{r} + \frac{1}{r}\frac{\partial v_r}{\partial\theta}\right)\hat{\mathbf{e}}_\varphi,$$

provided the system is spherically symmetric, which is the case with respect to the problem we focus on here. Recalling the useful relationship for the vorticity, Eq. (9), also has a component in the φ direction, we can simplify Eq. (2) to the following scalar form:

$$0 = \frac{\eta}{r\sin\theta}E^4\varphi + \eta'\nabla^2 v_\theta + \frac{\eta'}{r^2}\left(2\frac{\partial v_r}{\partial\theta} - \frac{v_\theta}{\sin^2\theta}\right) + \eta'\left(\frac{\partial^2 v_\theta}{\partial r^2} - \frac{1}{r}\frac{\partial^2 v_r}{\partial r\partial\theta}\right) + \eta''\left(\frac{\partial v_\theta}{\partial r} - \frac{v_\theta}{r} + \frac{1}{r}\frac{\partial v_r}{\partial\theta}\right). \tag{32}$$

The local viscosity and the corresponding derivatives are given by the Martin equation, Eq. (5), and the local concentration profile is defined by Eq. (4) [53]. Replacing the velocity components by $\varphi = f(r)\sin^2\theta$, we obtain a fourth-order ODE for the unknown radial function $f(r)$:

$$0 = f^{(4)} + \frac{2\eta'}{\eta}f''' - \left(\frac{4}{r^2} + \frac{2\eta'}{r\eta} - \frac{\eta''}{\eta}\right)f'' + \left(\frac{8}{r^3} - \frac{2\eta'}{r^2\eta} - \frac{2\eta''}{r\eta}\right)f' - \left(\frac{8}{r^4} - \frac{8\eta'}{r^3\eta} - \frac{2\eta''}{r^2\eta}\right)f \tag{33}$$

for $1 \leqslant r < \infty$. The corresponding no-slip and vanishing far-field boundary conditions are $f(1) = -1/2$, $f'(1) = -1$, $f/r^2 \to 0$, and $f'/r \to 0$ as $r \to \infty$. Equation (33) was solved by the Runge-Kutta integration method complemented by the shooting algorithm in order to obtain the unknown boundary conditions f'' and f''' at $r = 1$. From direct integration of the momentum equation, the pressure field can be expressed as

$$\frac{p(r,\theta)}{\cos\theta} = -\eta f''' - \eta' f'' + \left(\frac{2\eta}{r^2} + \frac{2\eta'}{r}\right)f' - \left(\frac{4\eta}{r^3} + \frac{2\eta'}{r^2}\right)f.$$

At the particle surface the pressure field reduces to $p(1,\theta) = -f'''(1)\cos\theta$. The normal stress

$$\sigma_{rr}(r,\theta) = -4\left(\frac{f'}{r^2} - \frac{2f}{r^3}\right)\cos\theta$$

vanishes at the particle surface, and the shear stress,

$$\sigma_{r\theta}(r,\theta) = \left(\frac{f''}{r} - \frac{2f'}{r^2} + \frac{2f}{r^3}\right)\sin\theta,$$

yields $\sigma_{r\theta}(1,\theta) = [1 + f''(1)]\sin\theta$. Finally by calculating the surface traction integration we conclude the translational correction factor g^t in the following compact form:

$$g^t = \frac{4}{9} + \frac{4}{9}f''(1) - \frac{2}{9}f'''(1). \tag{34}$$

The numerical procedure for finding g^t is straightforward. Given a characteristic depletion thickness d and the dimensionless bulk polymer concentration $[\eta]c_b$, shooting for the far-field boundary conditions to estimate $f''(1)$ and $f'''(1)$ gives one data point for g^t.

B. Rotational mode

The momentum equation for the shear-driven motion can be simplified to $\eta\nabla^2\mathbf{v} + \nabla\eta\cdot[\nabla\mathbf{v} + (\nabla\mathbf{v})^T] = 0$, and be reduced to a scalar form without using the stream function:

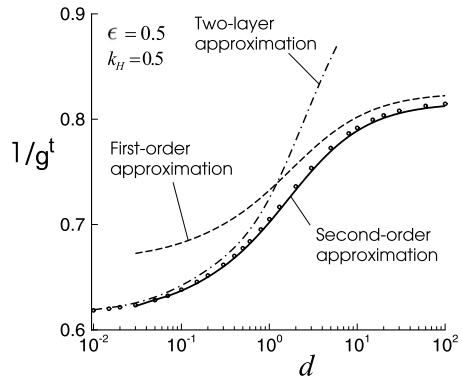

FIG. 3. Asymptotic (first order: dashed curve; second order: solid curve) solutions for the correction function g^t vs dimensionless depletion thickness d for $\epsilon = 0.5$ and $k_H = 0.5$. Results are compared with numerical results (circles) proposed in Sec. III and the two-layer (dash-dotted line) model [27].

$$0 = \frac{1}{r^2}\frac{\partial}{\partial r}\left(r^2\frac{\partial v_\varphi}{\partial r}\right) + \frac{1}{r^2\sin(\theta)}\frac{\partial}{\partial\theta}\left(\sin(\theta)\frac{\partial v_\varphi}{\partial\theta}\right) - \frac{v_\varphi}{r^2\sin^2\theta} + \frac{\eta'}{\eta}\left[r\frac{\partial}{\partial r}\left(\frac{v_\varphi}{r}\right)\right]. \tag{35}$$

By substituting $v_\varphi = w(r)\sin\theta$ into Eq. (35), we obtain the second-order ODE for the radial function $w(r)$:

$$0 = w'' + \left(\frac{2}{r} + \frac{\eta'}{\eta}\right)w' - \left(\frac{2}{r^2} + \frac{\eta'}{\eta r}\right)w, \tag{36}$$

where the corresponding no-slip and vanishing boundary conditions are $w(1) = 1$ and $w \to 0$ as $r \to \infty$. The final result for the surface shear stress is

$$\sigma_{\varphi r}(1,\theta) = [w'(1) - 1]\sin\theta. \tag{37}$$

From torque resistance we found the correction function

$$g^r = \frac{1}{3}[1 - w'(1)]. \tag{38}$$

Similar to the translational case, $w'(1)$ can be solved by the Runge-Kutta method and a shooting algorithm.

IV. RESULTS AND DISCUSSION

A. Model comparison

The numerical results from Eqs. (34) and (38) are computed over a wide range of polymer-to-sphere size for various concentrations including dilute and semidilute conditions, and are first used here to test the asymptotic solution in the dilute limit. In the dilute regime we apply the Huggins equation and choose $\epsilon = 0.5$ and $k_H = 0.5$. In that case $\eta_p/\eta_s \simeq 13/8$, so for $d \to 0$, the hydrodynamic resistance is determined by the bulk viscosity of polymer solutions and $1/g \simeq 0.615$. In Fig. 3 numerical results are compared for this condition with the asymptotic solution as a function of the relative depletion thickness d. The second-order asymptote coincides with the numerical prediction for the drag force

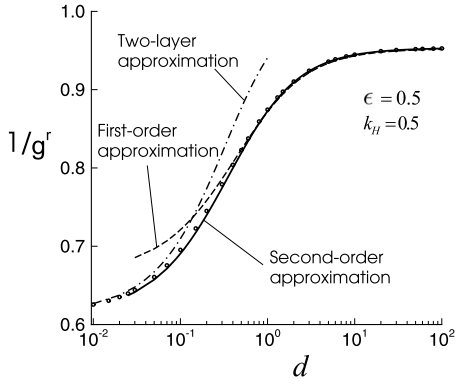

FIG. 4. Similar plot as in previous figure but for rotational motion.

and thus the long-time diffusivity for a translating sphere with a relatively large depletion thickness ranging from 0.03 up to an order of 100. The second-order approximation is almost indistinguishable from the "exact" numerical solution. However, the perturbation approximation is not applicable when the depletion layer is thinner than 0.03 for the case shown because the higher-order terms in Eq. (7a) are no longer uniform due to the large concentration gradient across the depletion layer.

Figure 3 includes a comparison with the two-layer approximation [26,27], which uses a step function to simplify the viscosity profile. The two-layer model well complements the perturbation analysis in the limit of very thin depletion layer, but starts to deviate from the current prediction when the depletion thickness approaches the particle size. Therefore a step function is only sufficient for predicting the resistance in the thin depletion layer regime. Beyond this regime, the two-layer model underpredicts the resistance significantly. An important aspect of the asymptotic analysis is to show that the retardation effect does not vanish even for values of d up to 100. The correction function g is always less than unity, implying the particle senses the increase of viscosity due to dissolved polymer chains even in case its size is much smaller than the suspending polymer chains. This fact is not captured by the two-layer model.

Similarly, the results are compared for the torque a rotating sphere experiences, shown in Fig. 4. The first-order approximation now already provides an excellent approximation when $d \geqslant 0.2$, implying that, unlike translational motion, rotational motion has a strong local effect and is less sensitive to the bulk viscosity. In the limit of thin depletion layers, the approximation for g^r is again better presented by the two-layer model [27]. When $d \to 0$, $\eta_{\text{eff}} \to \eta_p$, both $1/g^t$ and $1/g^r \to \eta_s/\eta_p \simeq 0.615$, and the hydrodynamic resistance is determined by the bulk viscosity of polymer solutions. Note that the numerical prediction has provided a trustable verification of the asymptotic model, but is not limited to dilute conditions. In Sec. IV B we will apply the same numerical procedure to reveal scaling behaviors for particle retardation in dilute and semidilute polymer solutions. Note that the numerical model here is limited to a spherical case when the convective effect is negligible so that the momentum equation can be simplified to an ODE.

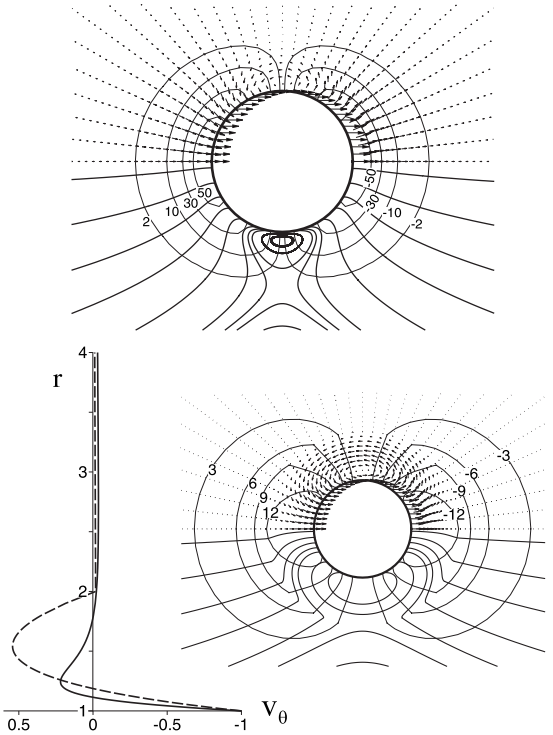

FIG. 5. Comparison of velocity vectors, streamlines, and normal stress fields for a translating sphere in a polymer solution based on numerical (top) and two-layer (bottom) models. Parameters used: $d=1$, $\lambda = \eta_s/\eta_p = 0.01$, $[\eta]c_b = 5.72$, and $k_H = 0.5$. The velocity profile v_θ at $1 \leqslant r \leqslant 4$ and $\theta = \pi/2$ reveals the flow field across the circulation region (solid curve: numerical model; dashed-curve: two-layer model).

We inspect the velocity and stress fields and observe the local effect near the particle surface in the semidilute regime, shown in Fig. 5. The bulk viscosity follows the Martin equation. Away from the depletion layer, the fluid is dragged by the moving particle and the velocity vanishes at the far field. In the representative case shown we compare current result with that from the two-layer model. By applying a continuous polymer concentration profile, the smooth streamlines (top) replace the kinky ones (bottom) and the circulation pattern is relatively weak and confined within the depletion layer, revealing an immediate effect corresponding to the continuous change of viscosity near the particle. The velocity profile shown (bottom left) is located at $\theta = \pi/2$. Near the particle surface the velocity gradient based on the numerical prediction (solid line) is larger than the two-layer approximation (dashed line), implying that the two-layer model previously developed [27] underestimates the shear resistance the sphere experiences. Combining with the total normal stress shown by contours, we confirm that the two-layer model underestimates the total resistance as mentioned above. For thin depletion layers the two-layer approach is, however, very accurate and it has the advantage that analytical expressions are available for the frictional coefficients. The velocity decaying rate is closely proportional to $1/r$ for both numerical and two-layer models. In the limit of very small d, the flow pattern is of course consistent with the pattern for the particle-driven Stokes flow in a homogeneous fluid.

B. Scaling behavior

Two most important factors that determine particle retardation effect are the apparent depletion thickness and the bulk polymer concentration, which are related to the polymer molar mass, particle size, polymer correlation length, solvent condition, and the intrinsic viscosity in many practical situations. To elaborate both asymptotic and numerical analyses we have proposed, it is important to connect these models to a useful correlation and scaling law. For this reason we attempt to describe our data using a generalized retardation factor [39]:

$$R = \exp(\alpha a^{\mu} c_b^{\nu}) \tag{39}$$

which is used often in the literature to interpret experimental data. Here R is an empirical retardation factor commonly used for determining an apparent transport property such as diffusivity or viscosity of polymer solutions, often linked to experimental data as $R=D_s/D=\eta/\eta_s$. Subscript s stands for pure solvent. In Eq. (39), α is the retardation coefficient, a is the particle radius, and c_b is the bulk polymer concentration. Coefficient α and exponential exponents μ and ν are empirical parameters. In dimensionless form, the stretched exponential function can be written as

$$\frac{1}{R} = \exp\left[-\alpha' \left(\frac{a}{d^*} \right)^{\mu'} (c_b[\eta])^{\nu'} \right], \tag{40}$$

where d^* is the dimensional depletion thickness appearing in this paper, and α', μ', and ν' are yet unknown parameters, which can be converted back to the original retardation coefficient α and the scaling exponents μ and ν, respectively. If the depletion thickness d^* is independent of c_b, the exponential exponents $\mu=\mu'$ and $\nu=\nu'$, and $\alpha=\alpha'(d^*)^{-\mu'}[\eta]^{\nu'}$ absorbs the rest of the transformation. If d^* depends on polymer concentration, the scaling exponent $\nu \neq \nu'$. Note that the inverse form of R is used later on because it fixes all $1/R$ values between 0 and 1, making it easier to present the scaling results.

The empirical retardation factor R has the same physical meaning as the correction function g^t or g^r, but mathematically they are not identical. This is because the upper and lower limits of the stretched exponential function are not bounded by the correct values while considering the depletion thickness influence (Fig. 6). The stretched exponential correlation can not be obtained directly from the theoretical results for the correction function due to the obvious mismatch in the limits. We thus propose a rescaling scheme to relate g to R in order to extract the useful R values from the numerical experiments. Without such a rescaling procedure, the dynamic similarity that predicts the particle retardation behaviors is unlikely to be established. This was done by comparing the limiting values of the theoretical results and the empirical form that covers a full range of particle size and polymer concentration. The proportional relation in Fig. 6 yields the rescaling scheme [54]:

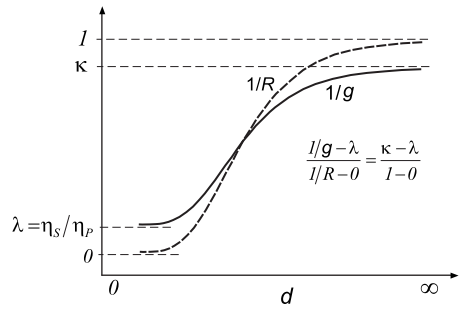

FIG. 6. A schematic plot showing the difference between the theoretical correction function g (with the correct upper and lower limits) and the empirical retardation factor R. The simple proportional relationship is used as the rescaling scheme.

$$\frac{1}{g} = \frac{1}{R}(\kappa - \lambda) + \lambda, \tag{41}$$

where the correction function g represents g^t and g^r for the decoupled translational and rotational motion. The lower bound λ corresponds to the colloid limit ($d \to 0$),

$$\lambda = \lim_{d \to 0} \frac{1}{g} = \frac{\eta_s}{\eta_p},$$

where the particle size is much larger than the polymer depletion thickness and the chain size or polymer correlation length. In fact, the correction function g in the colloid limit modifies the Stokes friction coefficient by converting the solvent viscosity η_s to the bulk viscosity η_p, an extreme case where the hydrodynamic resistance (retardation) reaches a maximum value at a given polymer concentration. On the other hand, the upper bound

$$\kappa = \lim_{d \to \infty} \frac{1}{g}$$

corresponds to the protein limit, where the statistically mean depletion layer extends over a much longer range and the particle is almost nonretarded (in which case, $g=1$). The quantity κ has a value very close to but less than unity. In the dilute limit, κ values corresponding to translational and rotational motion are given by the asymptotic solutions, Eqs. (24) and (31), respectively, with d approaching infinity.

Following the rescaling procedure, we found that the asymptotic results express an interesting self-similar retardation effect. Given $[\eta]c_b=0.1$, 0.3, 0.5, and 0.8, and a broad range of d from 0.03 to 300, we plot a number of points by calculating g^t and g^r from the second-order asymptotic solution, calculating the protein limit κ and colloid limit λ, and then substitute these values into R and finally introduce a global fit using Eq. (40).

We first focus on results for translational motion. A global fit of all results for g^t as a function of d for various concentrations using Eqs. (41) and (40) gives $\alpha'=0.818$, $\mu'=0.55$, and $\nu'=0.076$. The latter two indicate how strongly the retardation depends on depletion thickness and polymer concentration, respectively. Obviously the retardation effect is more sensitive to the apparent depletion thickness. Next we

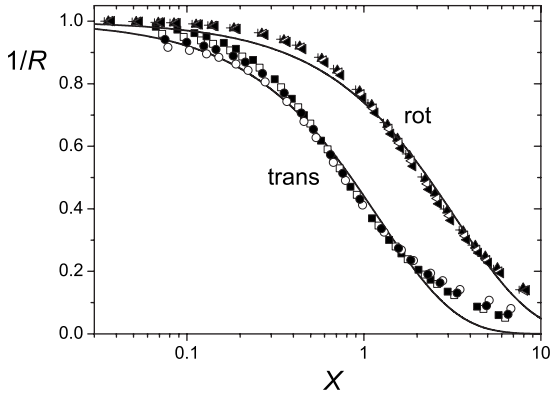

FIG. 7. A semilog plot of inverse retardation factor $1/R$ vs $X=(a/d^*)^{\mu'}(c_b[\eta])^{\nu'}$ in the dilute limit. Data points are from the second-order perturbation approximation. The solid lines are the best fits using Eq. (40) with $\alpha'=0.818$, $\mu'=0.55$, $\nu'=0.076$ for the translational motion, and $\alpha'=0.30076$, $\mu'=0.71$, $\nu'=0.046$ for the rotational motion.

plot all data points as a function of $X=(a/d^*)^{\mu'}(c_b[\eta])^{\nu'}$. As shown in Fig. 7 almost all data points fall onto a single curve. The solid curve follows the general expression for the retardation function $1/R=\exp(-\alpha' X)$. The agreement is excellent except for the regime close to the colloid limit where $d\to 0$. Such disagreement posts a question mark on using a universal stretched exponential function to describe experimental results under certain experimental conditions. Clearly, the exponential scaling well represents a global fit that can be used to quantify the retardation effect in the dilute regime. We emphasize that the rescaling step is essential in order to connect the numerically obtained g values to R, otherwise the data points will not fall onto a single curve. Many experimental works were in general designed for obtaining the correction function g by measuring the apparent transport property, we suggest that such data need to be rescaled before fitting the scaling exponents of the general retardation factor R.

Following the same procedure, we found that for rotational motion the retardation effect also fits into a stretched exponential scaling law with different coefficient and exponents. The best fit yields $\alpha'=0.30076$, $\mu'=0.71$, and $\nu'=0.046$. The obtained data for R for rotational motion are also plotted as a function of X in Fig. 7. It follows the change of the scaling exponents μ' and ν' has less impact on the retardation value R for given polymer conditions a/d^* and $c_b[\eta]$. Actually, it turns out the parameter α' is the primary factor to accommodate the change of flow pattern that influences the retardation effect. For rotational motion α' has a value of 0.3 which is relatively small compared with the value for translational motion, $\alpha'=0.818$, implying the rotational motion is much less retarded by the surrounding polymer chains. Physically this is because, unlike translational motion which has long-range effects, fluid flow induced by rotational motion decays quickly, and is confined within a much smaller space in which the particle does not fully sense the bulk viscosity. Therefore at the same polymer concentration the rotational motion is less sensitive to the bulk concentration and is less retarded than translational motion. We observed this already by comparing the first-order coefficients given by Eqs. (24) and (31). In the dilute limit, d^* is nearly independent of c_b, we can thus resume the corresponding scaling exponents $\mu=\mu'$ and $\nu=\nu'$ in the general retardation function.

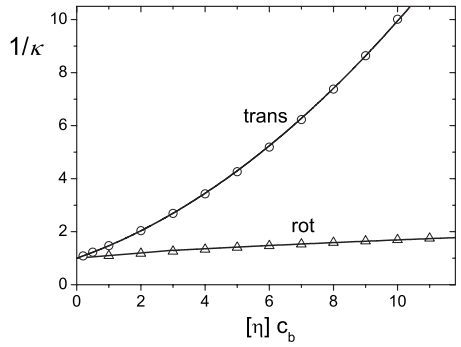

FIG. 8. Numerical evaluation of κ vs dimensionless concentration $[\eta]c_b$. The best fits for the translational and rotational motion follow $1/\kappa=g^t=1+(89/210)[\eta]c_b+0.047[\eta]^2c_b^2$ and $1/\kappa=g^r=1+0.1334([\eta]c_b)^{0.714}$, respectively.

In the semidilute regime, i.e., where the polymer concentration is beyond the overlap concentration c_b^* ($\approx 1/[\eta]$) and $\epsilon \geqslant 1$, we use the Martin equation for obtaining the bulk viscosity and the viscosity profile around a sphere. The upper bound for effective viscosity κ now needs to be calculated numerically by using the concentration profile:

$$\rho(r)=\left(\frac{r-1}{r}\right)^2, \tag{42}$$

which follows from Eq. (23) with $d\to\infty$. Here we separate the scaling law from the dilute regime because the apparent depletion thickness d^* is fundamentally different in both regimes. In the limit of dilute concentration, d^* is close to the polymer's gyration radius whereas in the semidilute regime d^* equals the polymer correlation length. Figure 8 shows the numerical results and best fits for κ. Using the upper bound κ and the numerical values of g^t and g^r we found the retardation factor R using Eq. (41).

In Fig. 9 we plot the resulting retardation function R as a function of X. A number of numerical data points are plotted for a broad range of polymer concentrations from $[\eta]c_b=2$ to 10, corresponding to a viscosity ratio $\eta_s/\eta_p=0.155-6.734\times 10^{-4}$, respectively, as follows from the Martin equation. For translational motion the best fit for the scaling law follows the solid line $1/R=\exp[-0.69(a/d^*)^{0.77}([\eta]c_b)^{0.44}]$. Under good solvent conditions where d^* scales as $d^*\sim c_b^{-3/4}$ [46], $\mu=\mu'$ and $\nu=(3/4)\mu'+\nu'\simeq 1.02$. These exponents resemble the nominal values of experimental observations collected in Ref. [39]. The dashed line that correlates the rotational retardation effect under the same polymer conditions follows $1/R=\exp[-0.325(a/d^*)^{0.67}([\eta]c_b)^{0.16}]$. The numerical results agree well with the scaling law when $d\geqslant 1$.

With respect to our earlier two-layer approximation [27] we have now used a realistic polymer concentration profile. We have thus obtained a more accurate description of the

frictional coefficient a sphere feels as it moves through a polymer solution. However, we have not yet considered the influence of convective effects; we assume a fixed depletion layer instead. Further experimental and analytical works are now in progress on resolving this problem.

V. SUMMARY

In this paper we presented an asymptotic and numerical analysis of tracer diffusivity in dilute and semidilute polymer solutions. Through straightforward hydrodynamic analysis including the dynamic depletion effect we found that retardation of particle diffusion is weakened by the depletion zone around the particle, implying a very small particle is allowed to diffuse almost freely through semidilute solutions of macromolecules, which is of great importance for many biophysical and biochemical applications. Our model provides a theoretical treatment of the semi-empirical stretched exponential retardation factor commonly employed in practice, and we propose a rescaling procedure to evaluate the retardation factor including the scaling exponents, which are consistent with the nominal values found in literature.

ACKNOWLEDGMENTS

T.-H.F. and B.X. are grateful for the financial support of this work from the University of Connecticut Research Foundation. R.T. wishes to thank M. G. McPhie, M. Fuchs, and M. G. H. Krüger for useful discussions.

APPENDIX

The integral form of Eq. (12) can be derived by multiplying a weighting function G to both sides of the equation and integrate them over the interval $[1,\infty)$, i.e.,

$$\int_1^\infty GLf_1 dr = \int_1^\infty Gh(r)dr.$$

Applying the Green identity the left-hand side of above equation becomes

$$\int_1^\infty GLf_1 dr = \int_1^\infty f_1 L^* G dr + \left\{ Gf_1''' - G'f_1'' + \left(G'' - \frac{4}{r^2}G\right)f_1' - \left[G''' - \left(\frac{4}{r^2}G\right)' - \frac{8}{r^3}G\right]f_1 \right\}_1^\infty, \tag{A1}$$

where $L \equiv L^*$. Clearly, the integral solution can be obtained by defining the weighting function as the Green function $G(r,\xi)$, which satisfies the singularly forced adjoint differential equation:

$$L^*(G) = \delta(r-\xi),$$

where δ is the Dirac delta function with field point located at the position r and the source point at ξ. We are interested in obtaining the Green function that satisfies the homogeneous boundary conditions:

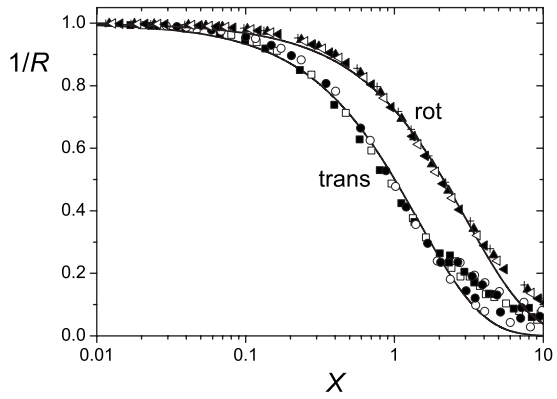

FIG. 9. Stretched exponential scaling laws for translational and rotational retardation factor R as a function of $X=(a/d^*)^{\mu'}(c_b[\eta])^{\nu'}$ in the semidilute regime. Data points are numerical results. The solid lines are the best fits using $\alpha'=0.69$, $\mu'=0.77$, $\nu'=0.44$ for the translational motion, and $\alpha'=0.325$, $\mu'=0.67$, $\nu'=0.16$ for the rotational motion.

$$G = 0 \quad \text{at } r = 1,$$

$$G' = 0 \quad \text{at } r = 1,$$

$$G/r^2 \to 0 \quad \text{as } r \to \infty,$$

$$G'/r \to 0 \quad \text{as } r \to \infty. \tag{A2}$$

From Eqs. (15) and (A2), one can assure that all of boundary terms on the right-hand side of Eq. (A1) vanish. Therefore the Green function integral solution for f_1 is

$$f_1(\xi) = \int_1^\infty G(r,\xi)h_1(r)dr$$

for $1 \leqslant r$, $\xi < \infty$. The remaining problem is to find the Green function. For the fourth-order system, $G(r,\xi)$ has continuous zeroth, first, and second derivatives with respect to the field parameter r, and has a discontinuity in the third derivative at $r=\xi$. The finite jump for the third derivative is determined by the forward and backward limits. By letting

$$G(r,\xi) = \begin{cases} G_1(r,\xi) & \text{for } 1 \leqslant r \leqslant \xi \\ G_2(r,\xi) & \text{for } \xi \leqslant r < \infty \end{cases},$$

the Green function has the following properties:

$$G_2(r,\xi) - G_1(r,\xi) = 0 \text{ at } r = \xi,$$

$$G_2'(r,\xi) - G_1'(r,\xi) = 0 \text{ at } r = \xi,$$

$$G_2''(r,\xi) - G_1''(r,\xi) = 0 \text{ at } r = \xi,$$

$$G_2'''(r \to \xi^+,\xi) - G_1'''(r \to \xi^-,\xi) = 1. \tag{A3}$$

To find G_1 and G_2 we apply the technique of variation of parameters [52]. First we express G_1 and G_2 as

$$G_1(r,\xi) = \sum_{i=1}^{4} \alpha_i(\xi) y_i(r), \quad G_2(r,\xi) = \sum_{i=1}^{4} \beta_i(\xi) y_i(r)$$

with $y_1 = r^4$, $y_2 = r^2$, $y_3 = r$, and $y_4 = 1/r$ being the bases of the general solution for the operator L. And then substituting G_1 and G_2 into Eqs. (A2) and (A3), the eight undetermined coefficient functions, $\alpha_1 - \alpha_4$ and $\beta_1 - \beta_4$, can be solved by a system of algebraic equations. After few matrix operations, we obtain G_1 and G_2 [Eq. (17)] in a symmetric form.

[1] R. Brown, *The Miscellaneous Botanical Works of Robert Brown*, edited by John J. Bennett (R. Hardwicke, London, 1866), Vol. 1.
[2] A. Einstein, *Investigations on the Theory of the Brownian Movement* (Dover, New York, 1956).
[3] M. Smoluchowski, Ann. Phys. **21**, 756 (1906).
[4] S. B. Zimmerman and A. P. Minton, Annu. Rev. Biophys. Biomol. Struct. **22**, 27 (1993).
[5] R. J. Ellis, Curr. Opin. Struct. Biol. **11**, 114 (2001).
[6] R. J. Ellis and A. P. Minton, Nature (London) **425**, 27 (2003).
[7] N. Kozer and G. Schreiber, J. Mol. Biol. **336**, 763 (2004).
[8] Y. Y. Kuttner, N. Kozer, E. Segal, G. Schreiber, and G. Haran, J. Am. Chem. Soc. **127**, 15138 (2005).
[9] M. S. Cheung, D. Klimov, and D. Thirumalai, Proc. Natl. Acad. Sci. U.S.A. **102**, 4753 (2005).
[10] G. G. Stokes, Trans. Cambridge Philos. Soc. **9**, 8 (1851).
[11] Z. Zapryanov and S. Tabakova, *Dynamics of Bubbles, Drops, and Rigid Particles* (Kluwer Academic Publishers, Dordrecht, 1999).
[12] P. J. W. Debye, *Polar Molecules* (Chemical Catalog Co., New York, 1929).
[13] Y. E. Solomentsev and J. L. Anderson, Phys. Fluids **8**, 1119 (1996).
[14] J. Szymański, A. Patkowski, A. Wilk, P. Garstecki, and R. Holyst, J. Phys. Chem. B **110**, 25593 (2006).
[15] T.-H. Lin and G. D. J. Phillies, J. Phys. Chem. **86**, 4073 (1982).
[16] A. M. Mastro and A. D. Keith, J. Cell Biol. **99**, 180 (1984).
[17] G. S. Ullmann, K. Ullmann, R. M. Lindner, and G. D. J. Phillies, J. Phys. Chem. **89**, 692 (1985).
[18] K. L. Yam, D. K. Anderson, and R. E. Buxbaum, Science **241**, 330 (1988).
[19] M. R. Wattenbarger, V. A. Bloomfield, Z. Bu, and P. S. Russo, Macromolecules **25**, 5263 (1992).
[20] O. Seksek, J. Biwersi, and A. S. Verkman, J. Cell Biol. **138**, 131 (1997).
[21] X. Ye, P. Tong, and L. J. Fetters, Macromolecules **31**, 5785 (1998).
[22] G. H. Koenderink, H. Zhang, D. G. A. L. Aarts, M. P. Lettinga, A. P. Philipse, and G. Nägele, Faraday Discuss. **123**, 1 (2002).
[23] Y. Cheng, R. K. Prud'homme, and J. L. Thomas, Macromolecules **35**, 8111 (2002).
[24] E. Dauty and A. S. Verkman, J. Mol. Recognit. **17**, 441 (2004).
[25] G. H. Koenderink, S. Sacanna, D. G. A. L. Aarts, and A. P. Philipse, Phys. Rev. E **69**, 021804 (2004).
[26] R. Tuinier, J. K. G. Dhont, and T.-H. Fan, Europhys. Lett. **75**, 929 (2006).
[27] T.-H. Fan, J. K. G. Dhont, and R. Tuinier, Phys. Rev. E **75**, 011803 (2007).
[28] S. Asakura and F. Oosawa, J. Polym. Sci. **22**, 1255 (1954).
[29] A. Vrij, Pure Appl. Chem. **48**, 471 (1976).
[30] R. Tuinier, G. A. Vliegenthart, and H. N. W. Lekkerkerker, J. Chem. Phys. **113**, 10768 (2000).
[31] R. Tuinier, D. G. A. L. Aarts, H. H. Wensink, and H. N. W. Lekkerkerker, Phys. Chem. Chem. Phys. **5**, 3707 (2003).
[32] R. B. Jones and G. S. Burfield, Physica A **113A**, 152 (1985).
[33] T. G. Mason and D. A. Weitz, Phys. Rev. Lett. **74**, 1250 (1995).
[34] J. C. Crocker, M. T. Valentine, E. R. Weeks, T. Gisler, P. D. Kaplan, A. G. Yodh, and D. A. Weitz, Phys. Rev. Lett. **85**, 888 (2000).
[35] A. J. Levine and T. C. Lubensky, Phys. Rev. Lett. **85**, 1774 (2000).
[36] A. G. Ogston, B. N. Preston, and J. D. Wells, Proc. R. Soc. London, Ser. A **333**, 297 (1973).
[37] R. I. Cukier, Macromolecules **17**, 252 (1984).
[38] K. L. Ngai and G. D. J. Phillies, J. Chem. Phys. **105**, 8385 (1996).
[39] T. Odijk, Biophys. J. **79**, 2314 (2000).
[40] K. Kang, J. Gapinski, M. P. Lettinga, J. Buitenhuis, G. Meier, M. Ratajczyk, J. K. G. Dhont, and A. Patkowski, J. Chem. Phys. **122**, 044905 (2005).
[41] K. Kang, A. Wilk, J. Buitenhuis, A. Patkowski, and J. K. G. Dhont, J. Chem. Phys. **124**, 044907 (2006).
[42] S. Broersma, J. Chem. Phys. **28**, 1158 (1958).
[43] S. Broersma, J. Chem. Phys. **30**, 707 (1959).
[44] J. Mathews, Phys. Fluids **21**, 876 (1978).
[45] F. Rodriguez, J. Polym. Sci., Polym. Lett. Ed. **11**, 485 (1973).
[46] P. G. de Gennes, *Scaling Concepts in Polymer Physics* (Cornell University Press, Ithaca, 1979).
[47] E. Eisenriegler, J. Chem. Phys. **79**, 1052 (1983).
[48] R. Tuinier and T. Taniguchi, J. Phys.: Condens. Matter **17**, L9 (2005).
[49] G. J. Fleer, A. M. Skvortsov, and R. Tuinier, Macromolecules **36**, 7857 (2003).
[50] H. Lamb, *Hydrodynamics* (Dover, New York, 1932).
[51] J. Happel and H. Brenner, *Low Reynolds Number Hydrodynamics* (Prentice-Hall, Englewood Cliffs, NJ, 1965).
[52] M. Bôcher, Ann. Math. **13**, 71 (1911).
[53] We wish to note that in principle *any* viscosity profile can be inserted into Eq. (32). This would allow us also to describe, for instance, diffusion of colloids plus brushes once the viscosity and concentration profiles in the brush layers are known.
[54] R. Tuinier and T.-H. Fan, Soft Matter (to be published).